UCRL-JC-129176
PREPRINT

Experimental Issues in *In-Situ* Synchrotron X-Ray Diffraction at High Pressure and Temperature by Using a Laser-Heated Diamond-Anvil Cell

C.S. Yoo
H. Cynn
A. Campbell
J.-Z. Hu

This paper was prepared for submittal to the
Materials Research Society 1997 Fall Meeting
Boston, MA
December 1-5, 1997

December 1997

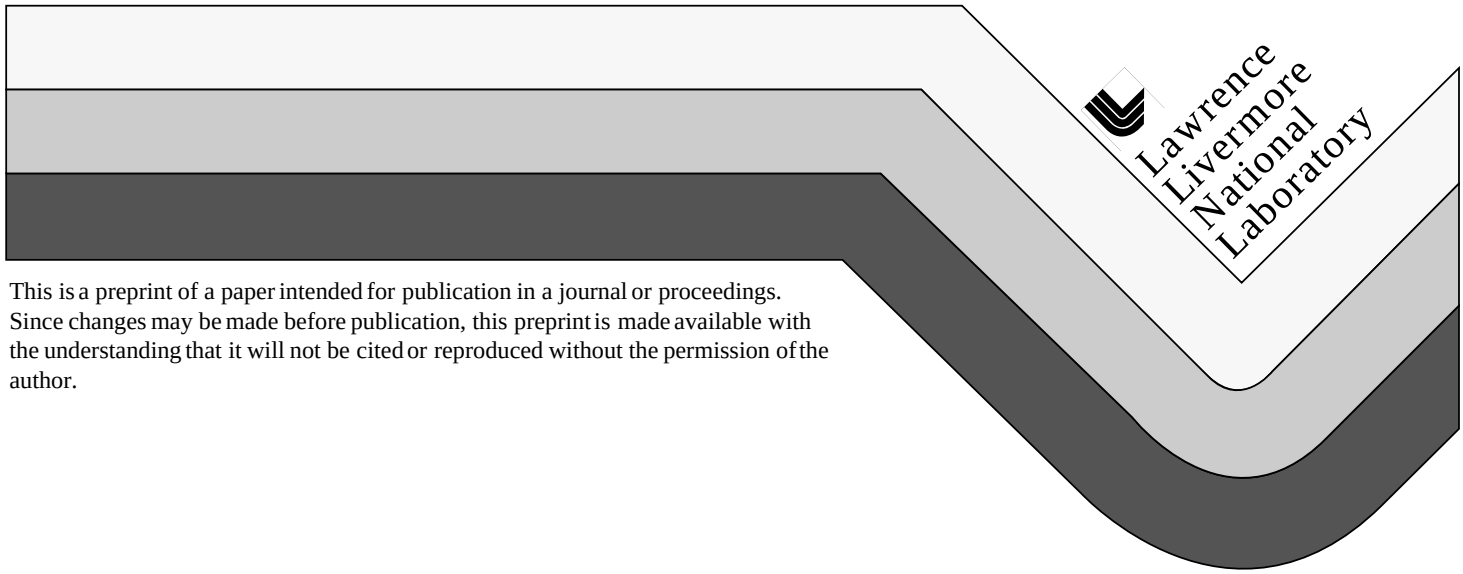

EXPERIMENTAL ISSUES IN *IN-SITU* SYNCHROTRON X-RAY DIFFRACTION AT HIGH PRESSURE AND TEMPERATURE BY USING A LASER-HEATED DIAMOND-ANVIL CELL

C. S. YOO*, H. CYNN*, A. Campbell**, J.-Z. HU**
* Lawrence Livermore National Laboratory, Livermore, CA 94551, yoo1@llnl.gov
* NSLS, Geophysical Laboratory, Carnegie Institute, Washington D.C. 20015

ABSTRACT

An integrated technique of diamond-anvil cell, laser-heating and synchrotron x-ray diffraction technologies is capable of structural investigation of condensed matter in an extended region of high pressures and temperatures above 100 GPa and 3000 K. The feasibility of this technique to obtain reliable data, however, strongly depends on several experimental issues, including optical and x-ray setups, thermal gradients, pressure homogeneity, preferred orientation, and chemical reaction. In this paper, we discuss about these experimental issues together with future perspectives of this technique for obtaining accurate data.

INTRODUCTION

Recent advances in *in-situ* x-ray diffraction studies of laser-heated materials in a diamond-anvil cell provide new information regarding the phase diagram of solids at high pressures and temperatures above 100 GPa (ca. 1 GPa=10^4 atmospheres) and 3000 K, far beyond the reach of other static high pressure technologies [1-4]. The concept of this x-ray/laser-heating experiment is relatively simple as illustrated in Fig 1. A small piece of thin iron foil is typically loaded in a diamond-anvil cell of the Mao-Bell type, together with a pressure medium such as Ar, LiF, Al_2O_3, MgO, and Ruby crystals. Because of the relatively large absorption coefficient of metal in infrared, a Nd:Yag laser lasing at 1.06 μm is typically used to heat the sample. A white (or monochromatic) x-ray beam from the synchrotron is coaxially aligned to the center of laser-heating spot and, then, the x-ray diffraction from the sample is recorded as a function of energy at a fixed 2Θ angle (or as a function of 2Θ using an area detector such as an image plate). The temperature of the sample is determined by measuring thermal emission from the laser heated area simultaneously with the x-ray measurements. The pressure of the sample is determined either from the equation of state of the sample or by Ruby luminescence method.

This diamond-anvil cell x-ray/laser-heating technique has demonstrated its feasibility for studies of melting, phase transition, phase diagram and materials characterizations in an extended region of pressures and temperatures. However, the technology is still in its infancy, evident from controversies existing in the experimental results [3-5], and the accuracy of the data is rather poor due to several issues associated with the experiments. The issues include (i) the optical and x-ray setups and alignment, (ii) temperature gradients in the x-rayed sample, (iii) pressure medium, sample, and pressure inhomogeneity, (iv) preferred orientation, and (v) chemical reactivity of the sample at high pressures and temperatures.

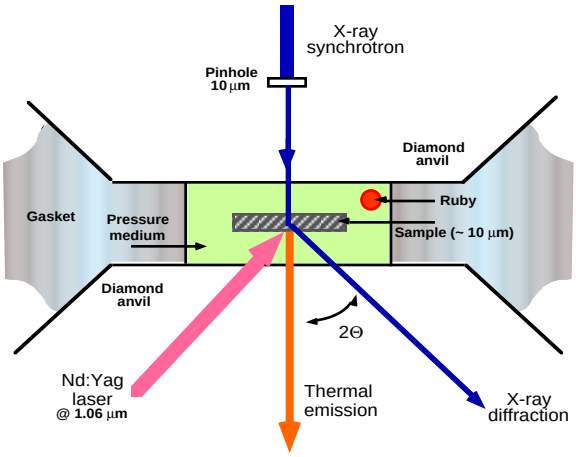

Figure 1. A simplified schematic view of in-situ DAC x-ray/laser-heating experiments.

In this paper, we will discuss about these issues and present a few feasible solutions to improve the accuracy of data, some of which have already been under development [6].

EXPERIMENTAL ISSUES

Optical Setup for DAC X-ray/Laser-heating Experiments

The optical setup for the DAC x-ray laser-heating experiment is shown in Fig 2. It consists of three components: (1) a Nd:Yag laser-heating system to heat the sample in a DAC, (2) a microscope system to measure temperature and view the sample for alignment and observation, and (3) synchrotron X-ray and an energy dispersive X-ray diffraction system.

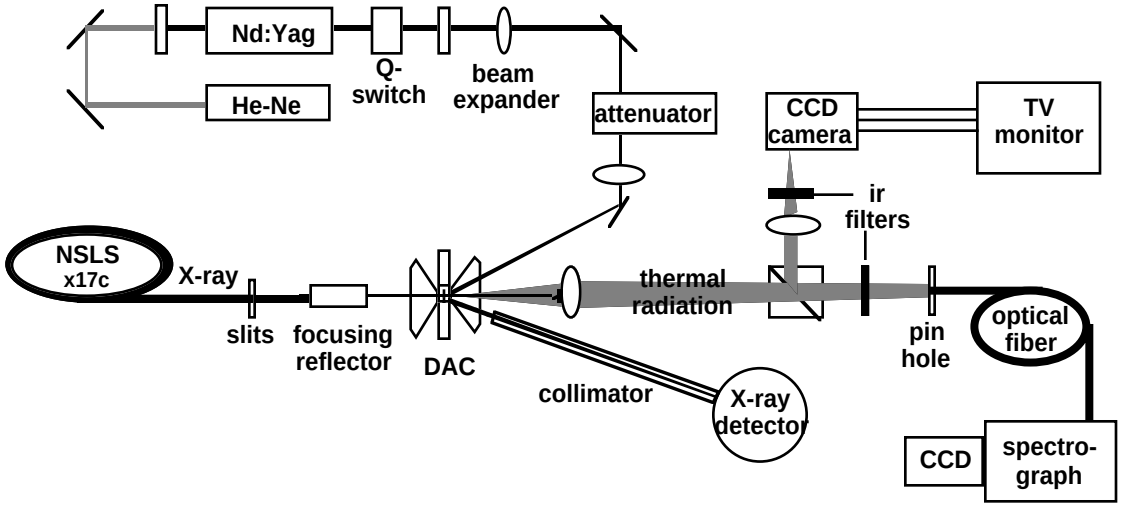

Figure 2. An optical setup used for the DAC X-ray, laser-heating experiments at the beamline X17C of the NSLS. The system consists of three parts including a Nd:Yag based laser-heating system, an EDXD system with partially focused synchrotron x-ray, and a microscope system for viewing and temperature measurements.

The Nd:Yag laser delivers the CW power to 19 W at TEM_{00} mode at 1.06 μm. The laser beam is first expanded by a 4x beam expander and is attenuated by an attenuator. Two types of attenuators have been used, either a polarizing element consisting of a polarizer beamsplitter with a half-wave plate or a broad band attenuator consisting of two pairs of counter-rotating wedged reflectors [7]. However, in many cases the laser power is also adjusted by altering the laser current. The laser beam is focused to the sample with an objective lens at approximately 30 degrees from a direction parallel to the X-ray beam. In this configuration the laser focus can be adjusted independently from the collecting optics to reduce thermal gradients within the laser spot. The laser light and the pump light are spatially filtered from the collecting optics. Note that no dichroic mirror, which would limit the spectral window to less than 700 nm, is needed to separate the laser light from the thermal emission. Only an infrared edge filter with a cutoff wavelength at 900 nm is used to separate the scattered laser light. A He-Ne laser is used for alignment of the Nd:Yag laser. In this experiment we used high power laser mirrors, each of which have dielectric high reflection coating for two wavelength at 1064 nm for the Nd:Yag laser and at 632 nm for the He-Ne laser.

Thermal emission from the sample is collimated by an objective lens (12x, Leitz) and then splits into two parts: 30 % to a CCD camera for sample viewing and 70 % to an optical fiber through a 100 μm pinhole for temperature measurements. The latter is obtained by dispersing thermal emission by a spectrograph (0.32 m, SPEX Ind.) and recorded in a two-dimensional CCD detector (LN-CCD, Princeton Instrument) with 1156 channels by 396 pixels. Because of the use of a refracting objective, there could be large chromatic aberration, particularly if the laser heating spot is smaller than a few to several μm. However, in the most of experiments reported here, the laser heating spot based on 90 % of the maximum temperature is near 30 μm or larger, and the chromatic aberration is not significant. Assuming a spectrograph slit opening of 10 μm or less, the spatial resolution of this microscopic system is limited by the spatial resolution of CCD pixels; that is, 22 μm which corresponds to 1.4 μm at the sample. The spectral resolution of the system is about 0.5 Å.

Because of significant thermal gradients across the laser heated area and a relatively large size of x-ray beam which will be discussed below, temperature has also been spatially resolved across the heated area for the latter part of this work. This was done by replacing the pinhole in the earlier setup by a multiple-core imaging fiber. In this setup an image from the fiber is transferred onto a slit of the spectrograph by using a spherical mirror. In this way one can adjust an effective f-number of the spectrograph to match with the fiber, and further correct stigmatic distortion of the spectrograph, particularly in a vertical direction, by rotating the mirror. The magnification of this imaging spectrograph was measured to be approximately one. Thermal emission is measured in every 27 μm-pixels within the laser heating area, representing an area of approximately 2.3 μm at the sample. However, because the diffraction limit of the objective is about 5 μm in the spectral region of interest, temperatures are calculated at every pixel by averaging over three pixels including two adjacent ones. Therefore, this system measures the temperature representing an area of 6.9 μm in diameter with a spatial resolution of 2.3 μm.

This study is based on the experiments performed on the beamline X17C at the NSLS, which produces white radiation from a wiggler insertion device. For the early part of this work we used unfocused x-ray beam. The size of the x-ray beam was typically reduced to 20 μm by 20 μm (or 10 μm by 10 μm for heavy Z elements) using two pairs of vertical and horizontal slits. The beam size was required to get a reasonable S/N ratio of 10-100 within a practical exposure time period of 5 to 10 minutes. For the later part of this study we focused the x-ray beam to reduce the beam size without loss of x-ray photons. This was done by using a Rh multilayer x-ray reflector which focuses the 70 μm beam to 5 μm in the vertical direction. The beam was unfocused in the horizontal direction remaining 20 μm as set by a pair of micro-slits. The vertical divergence of the beam on the beamline was about 0.5 mrad, and the size of the beam at the center of the sample

was measured to less than 20 μm by 7 μm by a knife-edge technique. Therefore, with this setup the horizontal beam size which is relatively large, could cause a large temperature gradient within the volume of the sample being x-rayed. This will be discussed in the next subsection. The use of an additional mirror in the horizontal direction should reduce the temperature gradient in a great deal; however, it has not been used due to the space limitation between the slit and DAC in the current setup at the X17C hutch.

The diffraction is typically measured at $2\Theta = 19^o$ or 21^o. In the setup shown in Fig 2 an angle smaller than 19^o is not feasible because of the physical interference with the objective lens of the microscope. However, smaller angles can be accessible by use of an additional turning mirror and mounting the microscope system in a vertical position. The energy dispersive x-ray system used here has previously been described in details [8].

The most tedious but crucial step in this work is to align the x-ray beam onto the center of the laser-heated spot and to the microscope. This is done in the following manner. (1) The center of the sample is aligned with respect to the 2Θ rotational axis of the diffractometer. (2) The x-ray beam is scanned across the sample to find its center and is moved to the center by traveling the x-ray slits. (3) The microscope with a pinhole is then aligned to the center of the sample. (4) Finally, the laser-heating spot is moved to the sample center. The positions for laser spot, sample, and pinhole can be reproduced within a few μm using a CCD camera and a high resolution television monitor. The position of the direct x-ray beam can be reproduced well within 5 μm. Therefore, in this setup the X-ray beam and laser-heating spot are coincident to within 5-8 μm.

Temperature Gradients

One of the most critical issues in the X-ray laser-heating experiment is large thermal gradients occurring in both radial and vertical directions of the laser heated sample. Those gradients arise from the facts that the laser-heated area is relatively small compared to the size of the x-ray beam and that the temperature is measured from a thin layer of the sample surface, yet the x-ray diffraction is obtained from the entire sample thickness. The temperature gradient in the radial direction can be reduced by minimizing the size of the X-ray beam and maximizing the diameter of the laser-heated area. The temperature gradient in the vertical direction can also be reduced by minimizing the thickness of the sample. However, in practice this is often not feasible in many materials with low x-ray absorption cross section including iron, because both of the above methods also reduce the intensity of x-ray diffraction. On the other hand, the sample can be heated from both front and back; however, this was not attempted in the present study because of relatively low intensity of laser and physical constraint of a diamond-anvil cell.

The temperature gradient can be measured or calculated. Figure 3 shows the temperature gradient in the radial direction of laser-heated iron at various degrees of heating. The smooth lines are the fits to the temperature profiles. The error bars in the figure represent the precision of the fitting procedure, but the actual uncertainty in the sample temperature could be substantially larger. For example, considering the uncertainty in the beam positioning and alignment 5-8 μm, the temperature measured at a given position could be off by 100 K at the maximum temperature of 2900 K in Fig 3. Furthermore, based on the size of the x-ray beam 20 μm by 20 μm, the temperature gradient within the X-ray illuminated portion of the sample could be as large as 250 K at 2900 K.

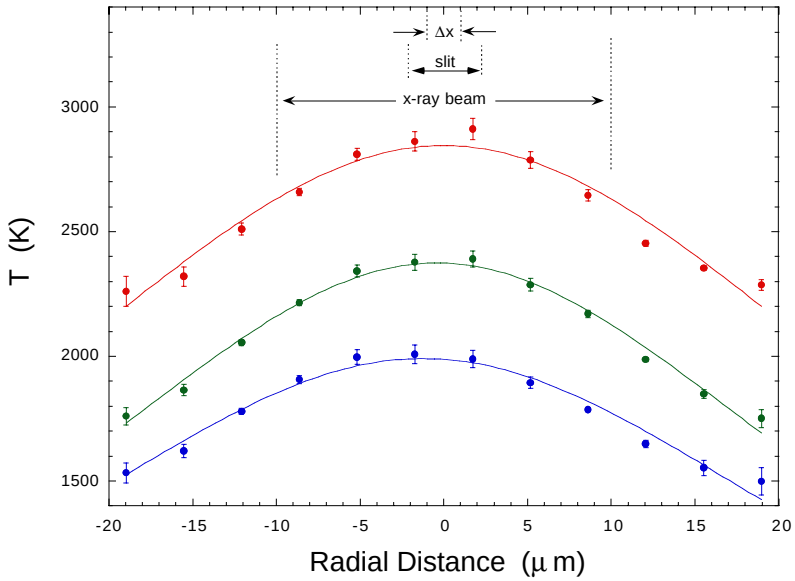

Figure 3. The temperature gradients measured along the radial direction of the laser heated iron sample at the designated temperatures at 96 GPa. The error bars represent the uncertainty in the fitting procedure and the smooth lines are the fits to the data using a Lorentzian band shape.

We have estimated the temperature gradient in the vertical direction by solving the thermal conduction equation [9]

$$\kappa \; d^2T/dq^2 = (1/\rho C)\, dT/dt + Q \qquad (1)$$

where κ, ρ and C are the thermal conductivity, density and heat capacity, respectively. Q represents the heat flux introduced from the laser. In this calculation we have assumed an 1-dimensional heat flow with a configuration that thin, 10 μm, iron foil is sandwiched between two slabs, each 20 μm thick, of Al_2O_3 in a diamond-anvil cell. The thermal parameters used in this calculation were estimated for values appropriate for 100 GPa [10]. The thermal conductivity and heat capacity of materials were, respectively, 100 W/m-K and 447 J/Kg-K for iron, 1300 W/m-K and 170 J/Kg-K for diamond and 38 W/m-K and 500 J/Kg-K for Al_2O_3. The effect of laser-heating is then introduced by a constant heat flux onto the central 20 μm in diameter area of the iron foil. For example, in the case of about 5 W of the laser power being used and a 70 % conversion of the radiation to thermal energy, the heat flux would be the order of $1.*10^{10}$ W/m^2.

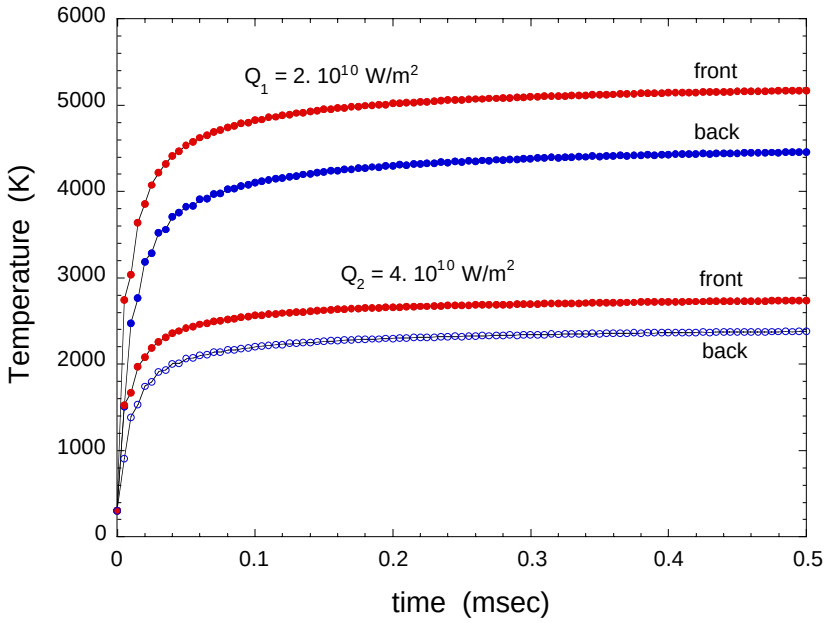

Figure 4. The temperature changes with time calculated across the iron sample at the center of the laser-heating spot at a heat flux of $2*10^{10}$ W/m^2 and $4*10^{10}$ W/m^2.

Figure 4 shows the temperature changes of iron at the front and back surfaces during the heating at the rate of $2*10^{10}$ W/m^2 (10 W) and $4*10^{10}$ W/m^2 (20 W). The temperature of the iron foil is rapidly increased during the first 100 μs heating and is then equilibrated during the next few 100 μs. The temperature of the directly heated, front surface of iron is approximately 10 % higher than that of the back, implying there could be a significant temperature gradient across the iron foil. Therefore, one should consider the temperature reported here to be somewhat higher than the actual one, and the diffraction pattern might exhibit some complication, particularly at the phase boundaries. However, we should note that the temperature difference calculated in Fig 5 represents an upper limit due to a highly polycrystallized nature of Al_2O_3, which will cause a lower thermal conductivity and a non-ideal thermal contact at the Fe/ Al_2O_3 and Al_2O_3/diamond interfaces, both of which result in an additional insulating effect on iron.

Sample and Pressure Medium

The powder samples of iron have not been used in this study because of the possibility of formation of thin iron oxide films and/or of adsorption of water, on an extremely large surface area. While the oxide film of powder samples might reduce the chemical reactivity of the sample with pressure medium at high pressures and temperatures, it could result in a large uncertainty in determining the transition temperatures. Therefore, in this study we use the foil samples. However, one should note that the foil samples typically exhibit the preferred orientation which could cause uncertainty in determining the crystal structure.

The ideal pressure medium should be a good thermal insulator and a low x-ray scatterer, provide a quasi-hydrostatic condition with a minimum pressure gradient, and be chemically inert at high temperatures and pressures. In practice, it is often difficult to find a pressure medium that satisfies all of these criteria. For example, LiF is a low Z-material providing reasonably quasi-hydrostatic conditions, but its high thermal conductivity limits the laser-heating experiments at

high pressures. Argon is chemically inert and also provides nearly hydrostatic conditions, but its high compressibility limits the laser-heating experiments above 40 GPa. Al_2O_3 has relatively low x-ray cross section, but it often causes highly non-hydrostatic pressures, particularly in the case of large grain ruby particles being used. Transition metal oxides like MgO are not chemically inert to an open shell transition metal like iron at high pressures and temperatures, as will be shown in the subsequent section.

In this study we have used Ar at low pressures below 40 GPa and a fine grain (1 μm) Al_2O_3 powder at higher pressures. A significant pressure drop was often observed; the pressure drops by as much as 50 % during a few cycles of the heating occur, when the iron sample is loaded with large grain single crystals, 10 to a few tens μm, of ruby. We consider this to be a stress relaxation effect during laser heating of the sample and the pressure medium. In contrast, fine 1-μm grain polycrystals of Al_2O_3 provide a relatively small pressure drop. It should also be mentioned that the extra layers of unconfined Al_2O_3 between the gasket and diamond-anvils often cause a significant pressure drop after several cycles of laser-heating and, therefore, should be avoided.

Preferred Orientations

The orientation of the sample strongly depends on various stress conditions introduced by non-hydrostatic pressures and high temperature gradient. A good example of stress-induced preferred orientation under uniaxial compression has been demonstrated in very recent x-ray experiments [11].

In this paper, we consider the preferred orientation induced by thermal stress of the laser-heated area at 59 GPa as shown in Fig 5. The iron sample, ~80 μm by 50 μm in size, was loaded together with fine Al_2O_3 powder in a 100 μm gasket hole mounted on a 300 μm diamond culet. Each spectra were obtained across the sample in every 10 μm increment after several cycles of heatings of the sample. Clearly, the heated area at the center of the sample can be immediately recognized by the preferred orientation along the 100 direction; whereas, the surrounding area shows the orientation along the 101 direction. The heated area is approximately 20-30 μm representing the approximate size of laser-heating spot. The peak positions of the diffraction patterns remain unchanged across the sample, representing that the pressure difference across the sample is not significant. Based on the equation of state of ε-Fe [12], the pressure across the sample differs by less than 5 GPa, which is nearly the same as the pressure gradient in the sample before heating. Therefore, it is not apparent that there has been any additional pressure change during heating.

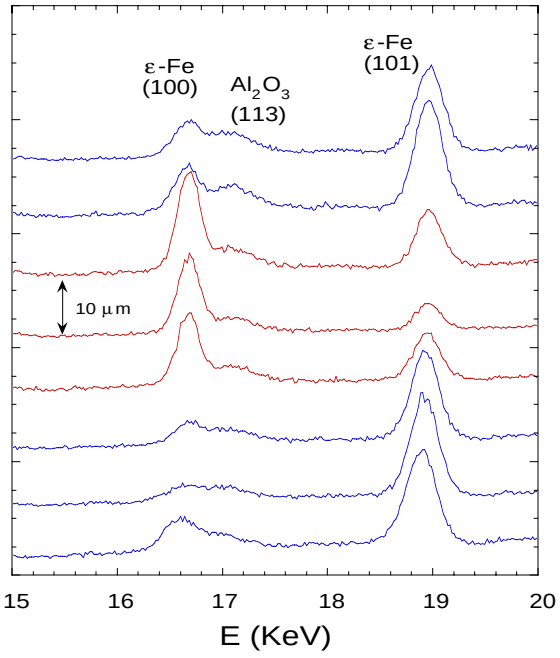

Figure 5. The X-ray diffraction pattern obtained from the sample after the laser-heating experiments showing the pressure distribution and preferred orientation across the sample at 59 GPa. Spectra were obtained for every 10 μm step.

Chemical reaction

The chemical reactivity of materials can substantially increase at high pressures and temperatures, particularly for those containing transition metals with an open electronic shell structure [13]. Moreover, reactivity is typically enhanced for the molten phase of materials due to increase of solubility. Therefore, it is not unusual to observe chemical reactions of the sample with the pressure medium, gasket, or even diamond anvils during the laser-heating experiments.

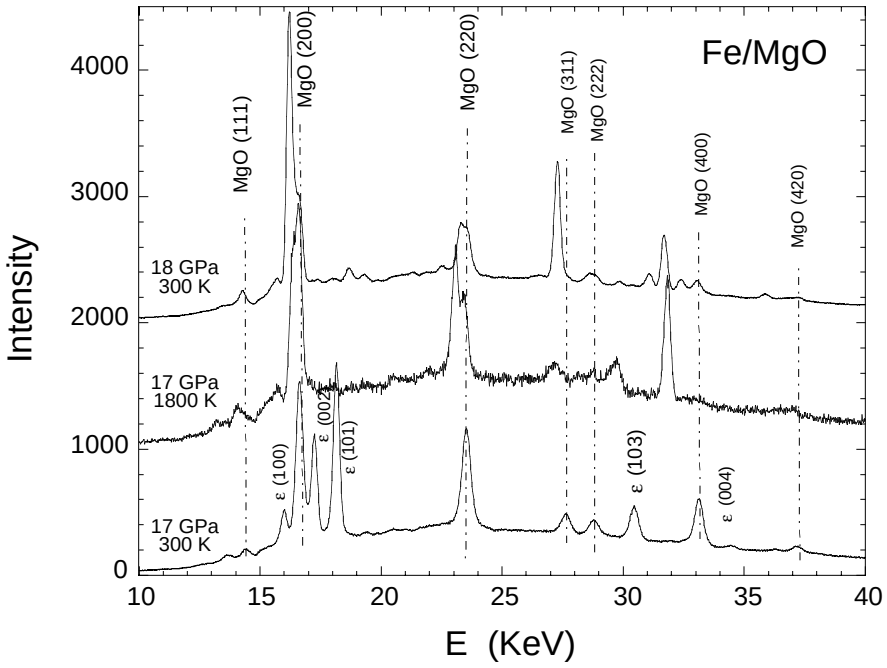

Figure 6. The X-ray diffraction patterns obtained from the laser heated iron in MgO, showing that iron reacts with MgO yielding ($Mg_{0.5}Fe_{0.5}$)O at high temperatures. The predicted crystal structures are found in Table I.

Figure 6 shows a typical example of iron reacting with MgO, a widely used pressure medium, yielding (Mg_xFe_y)O magnesiowustite. The diffraction before heating (the bottom spectrum) can easily be indexed in terms of fcc-MgO [14] and ε-Fe at 17 GPa as shown in Table I. During heating (the center), the diffraction lines of ε-Fe rapidly disappear as several new diffraction lines appear. After several heating cycles, the intensities of new reflections become larger than those of MgO, which can be quenched at low temperatures (see the top). The new diffraction lines show the same systematic pattern as fcc-MgO, but always appear at slightly lower energies than those of fcc-MgO. The new features are easily indexed as those of a fcc lattice, as shown in Table I. The best fit of this new material to a fcc structure yields the unit cell a = 4.156 Å, somewhat larger than that of MgO, a = 4.079 Å. In fact, the lattice of this new material is slightly larger than that of magnesiowustite ($Mg_{0.6}Fe_{0.4}$)O at 17 GPa, a = 4.136 Å, or same with that of ($Mg_{0.6}Fe_{0.4}$)O at 14 GPa [15]. Thus, it indicates that iron atoms have diffused into MgO during the heating. Assuming a linear expansion of the lattice with the number density of iron atoms substituted for magnesium, this material would represent a magnesiowustite of ($Mg_{0.5}Fe_{0.5}$)O. Therefore, we conclude that iron reacts with MgO at high temperatures, and

emphasize that one should be careful for choosing a chemically inert pressure medium at high pressures and temperatures.

Table I. X-ray diffraction pattern of iron in MgO before and after the laser heating experiments at 17 GPa showing that Fe reacts with MgO yielding (Mg_xFe_{1-x})O at high temperatures.

(a) Before heating

d_{obs} (Å)	d_{cal} (Å)	Δd (Å)	M (hkl)
2.353	2.357	0.004	MgO (111)
2.121	2.120	0.001	ε- Fe (100)
2.158	2.159	0.001	MgO (200)
1.965	1.983	0.018	ε- Fe (002)
1.871	1.869	0.002	ε- Fe (101)
1.448	1.448	0.000	ε- Fe (102)
	1.443	0.005	MgO (220)
1.227	1.231	0.004	MgO (220)
	1.224	0.007	ε- Fe (110)
1.178	1.178	0.000	MgO (220)
1.114	1.122	0.008	ε- Fe (103)
1.062	1.060	0.002	ε- Fe (220)
1.024	1.021	0.003	MgO (400)
0.984	0.991	0.007	ε- Fe (004)
0.935	0.937	0.002	MgO (331)
0.914	0.913	0.001	MgO (420)
0.833	0.827	0.006	ε- Fe (203)

ε-Fe: a = 2.4503 Å c = 3.9383 Å
c/a = 1.607 V = 6.166 cm^3/mol
MgO: a = 4.0819 Å V = 10.239 cm^3/mol

(b) After heating

d_{obs} (Å)	d_{cal} (Å)	Δd (Å)	M (hkl)
2.376	2.400	0.024	MFO (111)
	2.355	0.021	MgO (111)
2.093	2.093	0.000	MFO (200)
2.046	2.039	0.005	MgO (200)
1.883			ε- Fe (101)
1.819			
1.759			
1.456	1.469	0.013	MFO (220)
1.444	1.442	0.002	MgO (220)
1.279			
1.244	1.253	0.009	MFO (311)
1.228	1.230	0.002	MgO (311)
1.186	1.200	0.014	MFO (222)
1.176	1.177	0.001	MgO (222)
1.048	1.039	0.009	MFO (400)
1.027	1.020	0.007	MgO (400)
0.946	0.953	0.007	MFO (331)
0.911	0.912	0.001	MgO (420)

MgO: a = 4.0788 Å V = 10.216 cm^3/mol
MgFeO: a = 4.1562 Å
V = 10.809 cm3/mol

FUTURE PERSPECTIVES

It is apparent to obtain reliable data that one should carefully perform the diamond-anvil cell x-ray/laser-heating experiments and examine the systematics and reproducibility of the results. One of the most characteristic change in the diffraction during heating is a shift of the diffraction line, which could be taken as a measure of thermal expansivity. However, it is also true that the shift also strongly depends on the experimental variables such as hydrostaticity, inhomogeniety of pressure and temperature, stress relaxation, chemical reaction, mechanical stability of a DAC, and so on. Therefore, a typical strategy for performing a better characterized laser-heating measurement is to minimize the latter contributions, which typically occur irreversibly. This is illustrated in Fig 7, showing the diffraction patterns of iron in $Al_2 0_3$ obtained during laser heating at 96 GPa by using the system described earlier. The ε-Fe phase is evident from its characteristic triplet of 100, 101 and weak 002 reflections located in this pattern between 15 and 20 KeV. The feature from the pressure medium, $Al_2 0_3$, is weak but evident for the 113 line at 15.5 KeV [16]. Note that the thermal shift is nearly reversible during the heating cycle. The broadening of the diffraction bands is nearly negligible; the preferred orientation along the 100 direction is noted after the heating, consistent with the observation in Fig 5. The use of a 2D-x-ray detector such as an image-plate or a CCD should be encouraged to investigate the diffraction changes resulted from the preferred orientation, thermal stress, and non-hydrostatic stress induced strain of the sample in details.

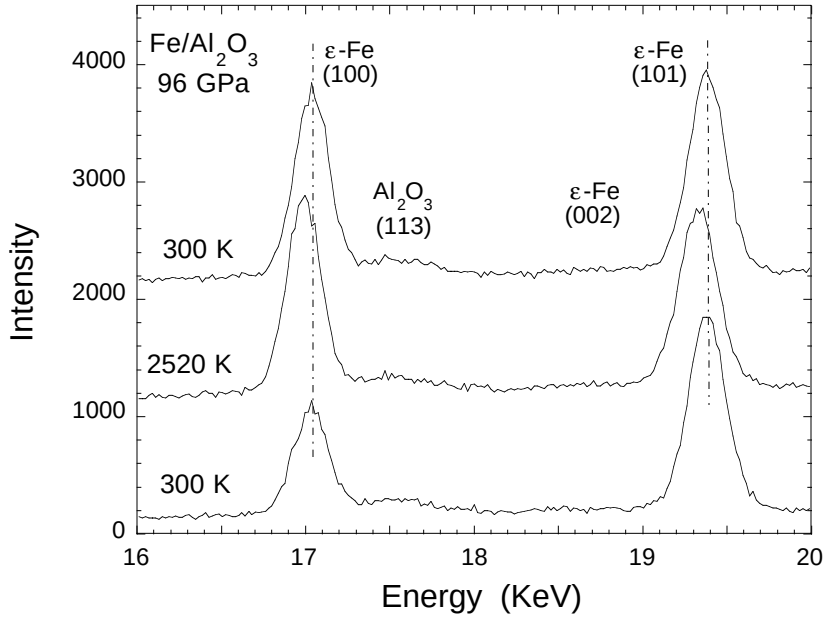

Figure 7. Typical X-ray diffraction patterns obtained from the laser heated iron at 96 GPa, showing totally reversible thermal shifts during laser heating cycles.

The present DAC x-ray/laser-heating technique is limited in a great deal by temperature gradients in the sample being x-rayed. This can be reduced in the radial direction by less tightly focusing the laser beam at higher power and in the axial direction by heating from both front and back of the sample. Recent advances in the YLF laser technology provide extremely high power lasers above 100 W with high beam stability and mode qualities [6]. Therefore, it is now possible to obtain a very homogenous large laser-heating spot with a minimum temperature gradient at the center. The added intensity of the laser makes also possible to heat the sample from both front and back sides, removing the axial temperature gradients. The dual-side heating, however, requires the modification of the cell and typically result in practical difficulty of the experiments (i.e., more optics and sophisticated alignment). Other solutions for the problem are to reduce (i) the size of x-

ray beam, preferably to less than 5 μm in diameter, (ii) the sample thickness less than 5 μm, and (iii) an x-ray exposure time; all of which require the substantial increase in x-ray intensity. Having 100-1000 times of the x-ray flux used in this study, it would be feasible to reduce the exposure time to an order of 10 seconds for a few μm-thick iron sample. In such a case, thermal gradients can be reduced within the uncertainty of temperature measurements 50 K and time-dependent temperature changes during x-ray measurements can be negligible. This condition can be achieved by use of intense x-ray beam from the 3rd generation synchrotron source and focusing the highly collimated beam from an undulator to less than 5 μm by 5 μm without losing much of the flux. Combining the intense 3rd generaltion synchrotron x-ray, high power laser, and 2D-detector, the x-ray/laser-heating technology should provide highly accurate PVT data within 1-2 %.

ACKNOWLEDGMENT

This study has been benefited from the use of synchrotron x-ray available at NSLS. We thank Mao and Hemley at GL-CI for numerous valuable discussions. We appreciate L. Wiley, B. Goodwin and C. Mailhiot at the LLNL for their support of the work. The LLNL part of this work has been supported by the LDRD 94-SR-042 and a Defense Program and performed under the auspices of the U.S. Department of Energy by Lawrence Livermore National Laboratory under contract number W-7405-ENG-48.

REFERENCES

1. R. Boehler, N. von Bargen, and A. Chopelas, J. Geophys. Res. **95**, 21731 (1990)

2. K. Brister and W. Bassett, Rev. Sci. Instrum. 66, 2698 (1995)

3. C.S. Yoo, J. Akella, A. Campbell, R. Hemley, and D. Mao, Science **270**, 1473 (1995)

4. D. Andrault, G. Fiquet, M. Kunz, F. Visocekas, D. Häusermann, Science **278**, 831 (1997).

5. S.K. Saxena, L.S. Dubrovinsky; C.S. Yoo, J. Akella, A.J. Campbell, H.K. Mao, and R.J. Hemley, Science **275**, 94 (1997)

6. G. Shen, T.S. Suffy, H.K. Mao, R. Hemley, M.L. Rivers, submitted (1997)

7. C.S. Yoo, C.S., J. Akella, and J.A. Moriarty, Phys. Rev. B **48**, 15529 (1993)

8. J. Hu, H.-K. Mao, J. Shu, and R.J. Hemley, in High pressure science and technology-1993, edited by S.C. Schmidt, J.W. Shaner, G.A. Samara, and M. Ross, part 1, pp 441, (AIP press, New York, 1994)

9. H.S. Carslaw and J.C. Jaeger in Conduction of Heat in Solids, (Clarendon, Oxford, 1959)

10. C.S. Yoo, N.C. Holmes, M. Ross, D.J. Webb, and C. Pike, Phys. Rev. Lett. **70**, 3931 (1993)

11. R.J. Hemley, H.K. Mao, G. Shen, J. Badro, P. Gillet, M. Hanfland, D. Häsermann, Science **276**, 1242 (1997)

12. H.K. Mao, Y. Wu, L.C. Chen, and J.F. Shu, and A.P. Jephcoat, J. Geophys. Res. **95**, 21737 (1990)

13. A.F. Wells, in Structural Inorganic Chemistry, Ch 27, pp 939, (Clarendon Press, Oxford, 1975)

14. T.S. Duffy, R.J. Hemley, and H.K. Mao, Phys. Rev. Lett. **74**, 1371 (1995)

15. Y. Fei, H.K. Mao, J. Shu, and J. Hu, Phys. Chem. Minerals, **18**, 416 (1992)

16. A.P. Jephcoat, R.J. Hemley and H.K. Mao, Physica B **150**, 115 (1988)

Technical Information Department • **Lawrence Livermore National Laboratory**
University of California • Livermore, California 94551